Structural and magnetic properties of semiepitaxial Co/Cr multilayers

Y. Henry, C. Mény, A. Dinia, and P. Panissod
Institut de Physique et de Chimie des Matériaux de Strasbourg, Groupe d'Etude des Matériaux Métalliques, Université Louis Pasteur, 4 rue Blaise Pascal, 67070 Strasbourg, France
(Received 23 December 1992)

The structural and magnetic properties of semiepitaxial Co/Cr multilayers have been studied using reflection high-energy electron diffraction (RHEED), nuclear magnetic resonance (NMR), and vibrating-sample magnetometry (VSM). A detailed analysis of the RHEED patterns observed during the growth shows that the Cr layers essentially consist of three types of distorted bcc (110) crystallites, one of them corresponding to the Nishiyama-Wassermann epitaxial relationship and the others to the Kurdjumov-Sachs one. From the resonance frequency of the NMR spectra main line we deduce the close-packed structure of the Co layers and using diffused-interface models we obtain the average concentration and magnetization profiles in the interfaces which are found to be 5 monolayers thick. The large intermixing is confirmed by a strong decrease of the measured saturation magnetization values as the Co-layer thickness decreases and is supposed to be responsible for the deviation from linearity, observed at small thicknesses, in the plot of the effective anisotropy per unit area versus Co-layer thickness.

I. INTRODUCTION

Owing to their high out-of-plane magnetic anisotropy mainly related to a columnar growth and a hcp structure with its c axis perpendicular to the surface, thin films of CoCr alloys have for a long time been considered as good media for perpendicular magnetic recording.[1,2] With the advent of deposition techniques allowing fine control over growth conditions, such a perpendicular anisotropy has been also sought and sometimes detected[3] in well-crystallized Co/Cr multilayers grown by various methods. Co and Cr have almost the same atomic size but very different bulk structures. Then epitaxial growth of multilayers using these two constituents can *a priori* lead to various epitaxial relationships between Co and Cr layers, depending essentially on the substrate orientation, deposition rate, and substrate temperature. Indeed, Co/Cr multilayers with different structures and textures have been observed.[3–5]

Most of the work on Co/Cr multilayers have pointed out that in these artificial systems, unlike in Co/Cu and Co/Au multilayers, sharp interfaces and good crystallographic quality are very difficult to obtain conjointly. Indeed the substrate temperature required to allow a suitable surface diffusion is often sufficient to give rise to a significant interdiffusion.[4,5] In many multilayers, the intermixing has been shown to be determinant for the magnetic properties such as saturation magnetization[4–6] and anisotropy.[6,7]

In this paper, we report on magnetic and structural properties of a series of Co/Cr multilayers grown by UHV e-beam evaporation. Their structural properties were studied by a detailed analysis of the reflection high-energy electron diffraction (RHEED) patterns observed during the deposition. This analysis reveals an original semiepitaxial growth of Cr on Co. The nanostructure of the buried Co layers and interfaces was characterized *ex situ* by nuclear magnetic resonance (NMR). The concentration and magnetization profiles in the diffused interfaces are deduced from the fits of the spectra. Finally, the magnetic properties which were determined from hysteresis loops are correlated to the structural ones.

II. GROWTH AND EXPERIMENTAL PROCEDURES

Semiepitaxial growth of Co/Cr multilayers was carried out in an e-beam evaporator RIBER system on mica substrates. Co and Cr layers were deposited at a rate of 3 Å/min out of an electron-beam hearth monitored by a quartz microbalance previously calibrated by Kiessig interferences through grazing x-ray diffraction. The base pressure before the film deposition was approximately 10^{-10} Torr while it was between 2 and 6×10^{-10} Torr during the deposition.

The mica substrates were freshly cleaved prior to introduction in the chamber and heated up to 500 °C *in situ* in order to drive off impurities. Then a 160 Å epitaxial hcp (0001) Ru buffer layer was grown at 500 °C in order to provide a smooth and clean single crystalline surface. Then the substrates were cooled down to 100 °C before multilayer growth. Results of preliminary growth tests have shown that the number of [Cr/Co] bilayers had to be limited to 10 and the Cr-layer thickness to 8 Å to ensure a good structural quality for all desired multilayers. In consequence, samples with Co-layer thickness varying from 8 to 32 Å and Cr-layer thickness fixed at 8 Å were prepared for this study. Finally, after growing sequential layers of Co and Cr, a 40 Å Cr protection layer was deposited.

The crystallographic structure of the films was examined, during all the growth, by RHEED observations at film surface with an electron-beam energy of 20 keV and, after the deposition, by NMR measurements performed at 1.5 K with a broadband pulsed NMR spectrometer. Vibrating-sample magnetometry was carried out at room temperature on 160 mm^2 samples with a Princeton Ap-

plied Research Model 155 magnetometer. Hysteresis loops were measured with applied fields up to 17 kOe, both parallel and perpendicular to the substrate plane.

III. RESULTS AND DISCUSSION

A. Structural properties

1. RHEED analysis

The crystallographic structure of the Co/Cr multilayers has been first examined by *in situ* reflection high-energy electron diffraction. The main features of the RHEED patterns observed during the growth are the following:

(i) the streaks become more and more spotty as the total thickness of the samples increases,

(ii) when Cr is deposited on hcp (0001) Ru buffer or on Co layers, a progressive splitting of the streaks located on each side of the specular one is observed,

(iii) this splitting progressively disappears when Cr is covered with Co.

In order to explain these observations, we propose the following analysis.

(i) Spotty streaks being characteristic of surface roughness, the first point shows that the layers become rougher as their distance from the buffer increases. The degradation of the RHEED patterns' quality essentially happens during the Cr deposition. This suggests a nucleation of Cr islands over the Co surface. This result is in agreement with that of a theorical model[8] which shows that a Cr monolayer does not wet a Co substrate (essentially due to the surface energy difference). Such a behavior has already been observed in sputtered Co/Cr multilayers by other authors.[4]

(ii) The second feature indicates that, in the chosen experimental conditions, Cr growth on hcp (0001) Ru or Co is not perfectly epitaxial. In order to explain the splitting and to translate it in structural terms, we have undertaken a detailed analysis of the RHEED patterns observed during the deposition of a 30 Å Cr layer on a hcp (0001) Co surface (with the same growth conditions as for the multilayers). For this study, the incidence angle of the electron beam has been highly increased ($\sim 4°$) with the aim of increasing 3D diffraction and obtaining structural information from the spot positions on the streaks.

For the lattice spacing calibration, a well-crystallized hcp (0001) Ru buffer layer has been used. Figure 1(a) shows the RHEED pattern of the (0001) Co surface observed in the [11$\bar{2}$0] direction before Cr deposition. All the following observations are made in that direction. The splitting, absent for Cr thicknesses lower than 2 Å [Fig. 1(b)], becomes clearly visible after the deposition of 6 Å [Fig. 1(c)]. Then it increases and reaches a stable value for Cr thicknesses larger than 12 Å [Fig. 1(d)]. As a result, two networks of equidistant spotty streaks, 1 and 2, respectively separated by the distances d_1 (the largest) and d_2 (the smallest), are observed on the screen (inset in Fig. 2). Figure 2 sums up the evolution of the splitting. It represents the variation of the d_2/d_1 ratio with the thickness of the evaporated Cr layer and it shows that, for Cr thicknesses larger than 12 Å, d_2/d_1 is constant and nearly equal to $\sqrt{3}/2$. When one looks at the spots intensity, it is clear that those of network 1 are less intense than those of network 2.

The limit value reached by the d_2/d_1 ratio on one hand, and the positions and intensities of the spots in the two networks of streaks on the other hand, are compati-

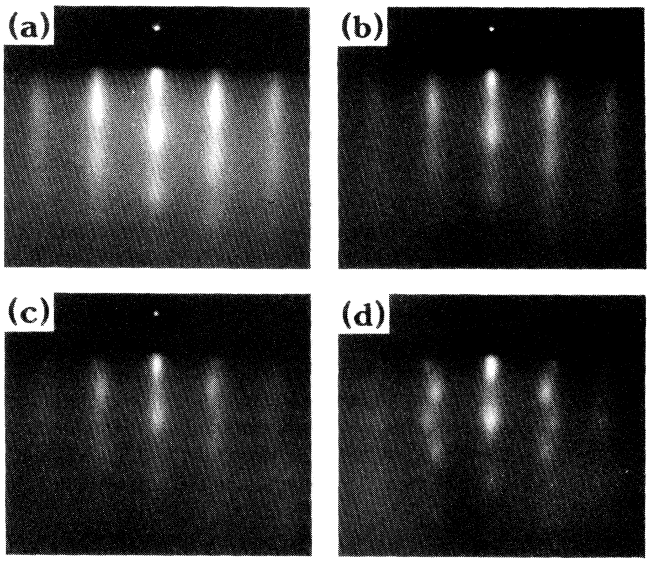

FIG. 1. Evolution of the RHEED patterns observed along the [11$\bar{2}$0] direction of a (0001) Co surface during the growth of a 30 Å Cr layer: (a) (0001) Co surface before Cr growth; (b) the pattern is unchanged after 2 Å Cr; (c) a streak splitting clearly appears after 6 Å Cr; (d) the splitting reaches a stable value for a Cr layer thicker than 12 Å.

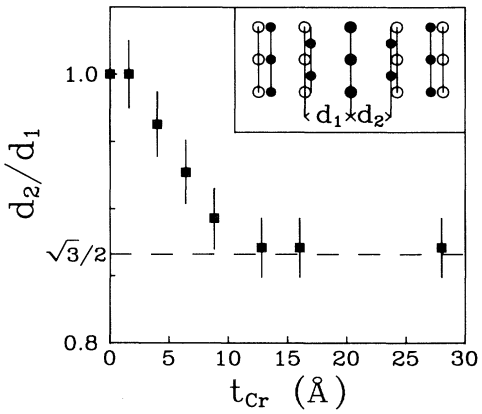

FIG. 2. Evolution of the splitting of the RHEED streaks observed along the [11$\bar{2}$0] direction of a (0001) Co surface during the growth of a 30 Å Cr layer. The d_2/d_1 ratio decreases and slowly relaxes to reach a constant value of about $\sqrt{3}/2$ for a Cr layer thicker than 12 Å. Inset: Schematic representation of the RHEED patterns observed in the [11$\bar{2}$0] direction of the (0001) Co surface after the deposition of 12 Å Cr. Two networks of equidistant spotty streaks separated by the distances d_1 and d_2 are visible.

ble with the superposition of the RHEED patterns along three different directions [A], [B], and [C] of a bcc (110) surface. These three directions are visualized in Fig. 3. The direction [A], for which the streaks are separated by $\sqrt{2}/a$, corresponds to network 1. Directions [B] and [C] give the same diffraction patterns. In consequence, these later are exactly superimposed and give network 2, in which the streaks are separated by $\sqrt{3}/(\sqrt{2}a)$. If we assume that the three directions have roughly the same weight, this exact superposition explains why the spots of this network are more intense than those of the other one, all nodes of the reciprocal lattice of a bcc lattice having the same structure factor. The bcc lattice parameters calculated from the distances d_1 and d_2 obtained for Cr thicknesses larger than 12 Å and using the (0001) Ru buffer layer as a reference are respectively, 2.875±0.073 Å and 2.890±0.079 Å. These values are in very good agreement with the parameter of the bulk bcc Cr ($a_{Cr}=2.884$ Å).

The evolution of the lattice spacings a_1 and a_2 corresponding to the distances d_1 and d_2 is reported in Fig. 4. The persistance of the sixfold in-plane symmetry during the deposition of the first 2 Å has two possible origins. One of them is a pseudomorphic growth, on the Co surface, of the first Cr monolayer which could be strained in the underlying close-packed structure. The other explanation is that pseudomorphism does not occur and the unchanged RHEED patterns are due to interdiffusion which results in a close-packed CoCr alloy. Other observations, which we will discuss later, favor the latter explanation. Figure 4 shows that beyond 2 Å, Cr progressively relaxes towards its bulk structure. The growth is then semiepitaxial and gives rise to three types of distorted bcc (110) crystallites associated with the three superimposed RHEED patterns. For a Cr layer thicker than 12 Å, the surface is completely relaxed and the crystallites' structure is perfectly bcc (110) as shown by the

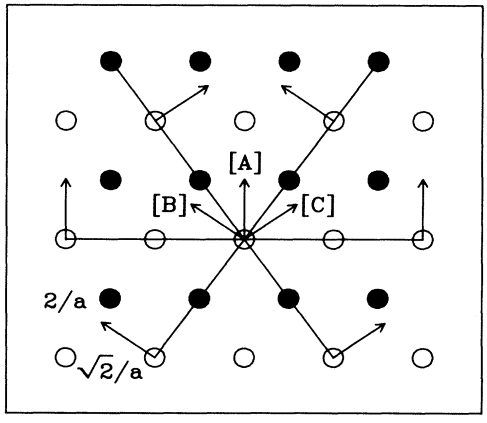

FIG. 3. Projection of the reciprocal lattice of a bcc structure on the (110) plane. Open circles stand for nodes at level 0, $\sqrt{2}/a$, $2\sqrt{2}/a\ldots$, whereas full circles represent nodes at level $\sqrt{2}/(2a)$, $3\sqrt{2}/(2a)$, $5\sqrt{2}/(2a)\ldots$. The superposition of the RHEED patterns along the [A], [B], and [C] directions is similar to the figures observed in the [11$\bar{2}$0] direction of the (0001) Co surface at the end of the 30 Å Cr-layer growth.

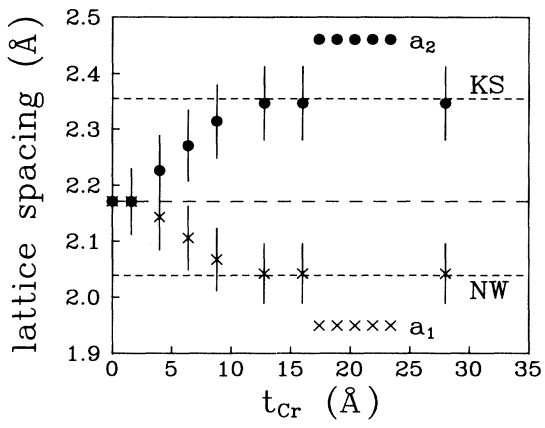

FIG. 4. Evolution with the Cr thickness of the lattice spacings a_1 (crosses) and a_2 (circles) calculated from the distances d_1 and d_2. These lattice spacings slowly relax and, for a Cr layer thicker than 12 Å, reach constant values which are those expected for the Nishiyama-Wasserman (NW) and Kurdjumov-Sachs (KS) epitaxial relationships (2.039 and 2.355 Å, respectively).

stacking parameter obtained from the vertical distance between spots $a_3=2.074\pm0.054$ Å, which is close to the bulk value $a_{Cr}/\sqrt{2}=2.039$ Å.

In bcc (110)/fcc (111) [or hcp (0001)] interface, two kinds of epitaxial orientation relationships are well known. These are the Nishiyama-Wasserman (NW)[9,10] and the Kurdjumov-Sachs (KS)[11] relationships. Both minimize the interfacial energy keeping the densest atomic rows parallel. They can be described using two parameters:[12] the atomic diameter ratio of bcc to fcc (or hcp), $\alpha=d_{bcc}/d_{fcc}$ (or $\alpha=d_{bcc}/d_{hcp}$) and the angle ϑ between the $[001]_{bcc}$ and the $[1\bar{1}0]_{fcc}$ (or $[11\bar{2}0]_{hcp}$) directions. These parameters (α,ϑ) are (1.061, 0°) for the NW relationship and (0.919, ±5.26°) for the KS one. The Cr (110)/Co (111) [or Co (0001)] interface which we are dealing with is characterized by $\alpha=0.996$. This value lies between 0.919 and 1.061. Then, since none of the two relationships is really favored, it would not be surprising to have crystallites related to the two kinds of epitaxial relationships. Their presence is actually confirmed in Fig. 4 which shows that, after the structural relaxation, the measured lattice spacings a_1 and a_2 are those expected for the NW and KS orientations ($a_{Cr}/\sqrt{2}=2.039$ Å and $2a_{Cr}/\sqrt{6}=2.355$ Å, respectively). Therefore, crystallites corresponding to network 1 are of the NW type where Cr $[001]_{bcc}$ atomic rows are parallel to Co $[1\bar{1}0]_{fcc}$ (or $[11\bar{2}0]_{hcp}$) ones, while the two variant crystallites corresponding to network 2 are of the KS type with Cr $[1\bar{1}1]_{bcc}\|$Co $[10\bar{1}]_{fcc}$ (or Co $[01\bar{1}0]_{hcp}$) for $\vartheta=-5.26°$ and Cr $[\bar{1}11]_{bcc}\|$Co $[0\bar{1}1]_{fcc}$ (or Co $[10\bar{1}0]_{hcp}$) for $\vartheta=5.26°$ (Fig. 5). Finally, we can conclude that the 30 Å Cr layer is essentially built from one close-packed monolayer covered by three kinds of distorted bcc (110) crystallites. This distorted bcc (110) structure is certainly that of the Cr layers which constitute the multilayers.

(iii) We now turn our attention to the third main feature. The progressive disappearance of the streaks'

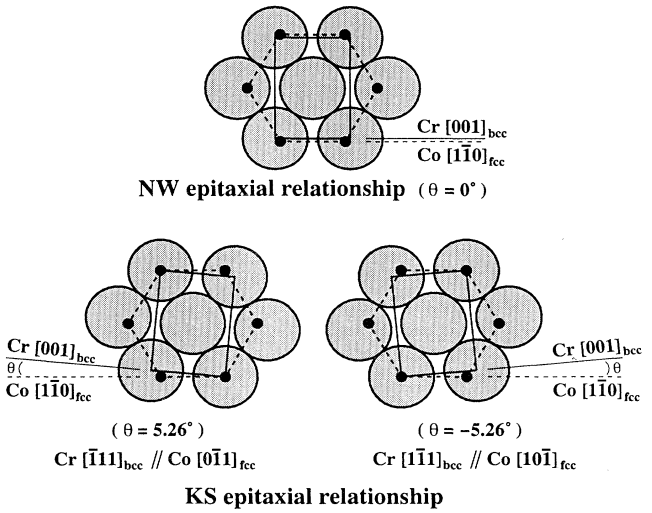

FIG. 5. Schematic representation of the bcc (110) Cr mesh (solid lines and shaded circles) on the fcc (111) or hcp (0001) Co mesh (dashed lines and dark circles) in the Nishiyama-Wasserman and Kurdjumov-Sachs orientations.

splitting indicates that Co grown on the strained bcc (110) Cr surfaces tends to recover a structure with a sixfold in-plane symmetry i.e., a fcc (111) or a hcp (0001) structure. Unfortunately, the RHEED patterns that we have observed during the Co deposition do not provide any information about the Co stacking in the multilayers. As a result, they do not allow the determination of the real structure among the two possibilities for the relaxed part of the Co layers or to know if the atoms which constitute the nonrelaxed part are in a bcc-like or in a close-packed-like strained structure.

Actually, the behavior described in (ii) and (iii) only corresponds to the growth of the early [Cr/Co] bilayers. Indeed, the split RHEED streaks remain visible longer and longer during the Co deposition as the number of bilayers increases. As a consequence, even if the sixfold in-plane symmetry is well restored at the end of the first and second bilayers of all samples, the only multilayer which still presents RHEED patterns characteristic of a surface close-packed structure after the deposition of the 10th bilayer is that with the 32 Å Co layers. For others, the splitting does not entirely disappear after a number of bilayers which decreases as t_{Co} decreases. Then Co atoms located in these regions are in the same structure as that of the nonrelaxed part described earlier. These observations suggest that Cr would progressively tend to impose its bcc structure made up of NW and KS crystallites if the Cr layers were thick enough to allow a complete structural relaxation.

2. *Nuclear magnetic resonance*

Zero-field ^{59}Co NMR spectra have been performed at 1.5 K using an automated frequency scanning broadband spectrometer with phase coherent detection. The spectra are corrected for the frequency-dependent enhancement factor and the ω^2 dependence of the NMR signal.

The NMR spectra of the samples with a Co layer thickness of 16, 24, and 32 Å of Co are shown in Fig. 6; no NMR signal could be observed for the smallest Co thickness of 8 Å. Even if the RHEED analysis shows that the structure of the close-packed Co planes is distorted in the last Co layers, there is no evidence on the NMR spectra for the presence of bulk bcc Co (main resonance line lying at 198 MHz, Ref. 13). This indicates that Co layers are still dominantly close packed though there could be a small bcc Co contribution to the low-frequency tail of the main NMR line. The observed frequency of the main line (220 MHz) is intermediate between the bulk fcc Co NMR frequency (217 NHz) and the bulk hcp Co frequency (228 MHz when magnetization lies in the [0001] plane). Since this intermediate frequency does not depend on the Co-layer thickness, it cannot be attributed to lattice strains which are shown to relax progressively. However, it has been shown[14] that stacking faults give rise to NMR lines lying between the fcc and hcp Co lines; hence the frequency of the main line suggests that many Co atoms are situated in layers where the two kinds of stacking (*ABA* and *ABC*) are intimately intermixed. The extended tail below the main line originates from Co atoms at the interfaces of the Co and Cr layers; indeed the vicinity of Cr atoms depresses the Co resonance frequency[14] and Co atoms with at least one Cr nearest neighbor contribute to this tail. As can be seen in Fig. 6(a), the low-frequency part of the spectra in the 24 and 32 Å Co thick samples are superimposed; this shows that the interfaces of the two samples have the same topology. The interface spectrum of the 16 Å Co thick sample looks slightly different, which is discussed in the next paragraph.

From the thickness dependence of the main Co line intensity,[15] the amount of Co atoms alloyed with Cr at the interfaces is estimated to have an equivalent Co thickness of about 11 Å in each Co layer. This large value is consistent with the fact that no signal could be observed in the 8 Å Co thick sample; the Co layers in this sample are alloyed to the core with Cr and they are too weakly magnetic to yield a significant NMR signal in the observation

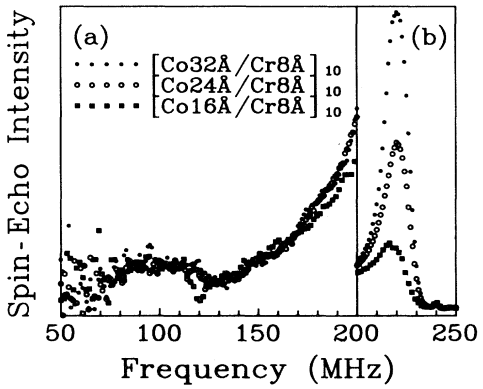

FIG. 6. ^{59}Co NMR spectra of the [Cr(8 Å)/Co(t_{Co} Å)]$_{10}$ multilayers with t_{Co} = 16, 24, and 32 Å. The low-frequency side (a) shows the interfacial part of the spectra (magnification is 4). The high-frequency side (b) shows the increase of the bulk-line intensity with the increase of the Co-layer thickness.

frequency range. The large amount of Co in the mixed interfaces can also explain why the shape of the 16 Å Co thick spectrum is different from the two other spectra. In this sample, the Co layers contain only 5 Å (~2 atomic layers) of unalloyed Co; in principle this would be the thinnest Co layer that exhibits the same interface spectrum as 24 and 32 Å thick layers. However, the layers are not perfectly flat and, from place to place, there is only one full Co monolayer left where Co atoms have Cr neighbors in both adjacent planes. This explains the decrease of intensity not only of the main line but of the upper frequency range of the interface spectrum as compared to spectra observed in the two other samples.

In order to gain more detailed information on the topology of the interfaces, we have tried to model the interface spectra. As already discussed in Refs. 15 and 16, the basis for interface spectra modeling is the shift of the Co NMR frequency resulting from the substitution of an alien element for Co in the nearest-neighbor shell; this shift gives rise to a succession of satellites to the bulk line separated by a gap which was found to be 32 MHz in reference CoCr bulk alloys. However, unlike in the most studied CoCu system, our study of CoCr alloys[14] has shown a significant influence of further neighbor shells on the NMR frequency; indeed, in these alloys, the frequency of the main line (Co with no Cr nearest neighbors) decreases strongly (2 MHz per percent of Cr) with increasing Cr content. Hence, beside the nearest-neighbor shell composition, our models must also take into account the influence of a local Cr concentration.

Considering the large amount of Co atoms in the interface, we have used diffused interface models where the interface consists of a succession of two-dimensional random alloys. Unlike that noted in Ref. 16, no *a priori* concentration profile was assumed but rather the Cr concentrations in each atomic layer of the half multilayer period are left free (with the constraint of a monotonic concentration profile). As the NMR spectrum averages over all interfaces in the structure, no information can be obtained on a possible asymmetry of the Co/Cr vs Cr/Co interfaces. The reconstructed spectrum consists of a sum of spectra, arising from Co nuclei in individual atomic planes, the position of which depends on a local Cr concentration to be defined, the shape of which reflects the occurrence probability of the various nearest-neighbor configurations (i.e., results from the actual composition of the plane and those of its adjacent planes). Hence the main parameters of the models are the Cr concentrations in the mixed atomic planes (at most 5); secondary parameters are the intensity corresponding to a full Co plane, the NMR frequency of the inner (bulk like) Co planes, and a broadening factor for the lines. However, two questions are still open. (i) Are the figures for the Co NMR frequency shifts in bulk alloys (a gap of −32 MHz per Cr nearest neighbor and an overall shift of −2 MHz per percent of Cr content) applicable to the case of a large concentration gradient? (ii) Which local concentration should be used to compute the overall shift of the spectrum from an individual plane?

As for the frequency shifts, they were either constrained to the alloy values or freed in the fit. Actually, in all free fits, the overall frequency shift with local composition always returned to the alloy value of −2 MHz per percent Cr; therefore this parameter will not be discussed any longer in the following. An example of a reconstructed spectrum where the gap between the satellites was constrained to the alloy value is shown in Fig. 7(a); although it reproduces the general shape of the spectrum, the detailed structures close to the main line are not well reproduced. A reconstruction obtained with a fit where the gap was freed is shown in Fig. 7(b). In this case the detailed features of the spectrum are very well reproduced and the adjusted gap value is then about 20 MHz. This value is much lower than in the alloys and needs to be discussed. In his study of a diluted $Co_{0.995}Cr_{0.005}$ hcp alloy, Kawakami[17] has already observed two satellites of equal intensity 41 and 22 MHz below the main line, which he has attributed both to the presence of one Cr nearest neighbor; considering the anisotropy of hcp Co, the frequency difference was explained by the different position of the Cr atom either in the same [0001] plane as the Co nucleus or in one of the adjacent planes. Our study of more concentrated alloys has shown that these two satellites merge into a broad one about halfway between the two. Since there is a concentration gradient in the multilayers, configurations with a given number of Cr neighbors are not isotropic on average (unlike in alloys) but have a dominant contribution, not from the plane of the observed Co nucleus, but from the adjacent plane on the Cr-rich side. Hence the 22 MHz frequency gap observed by Kawakami, which is close to the one obtained by our fit of the multilayer spectra, could be attributed to Co atoms with Cr impurities out of their [0001] plane.

In order to see the influence of the choice of the local

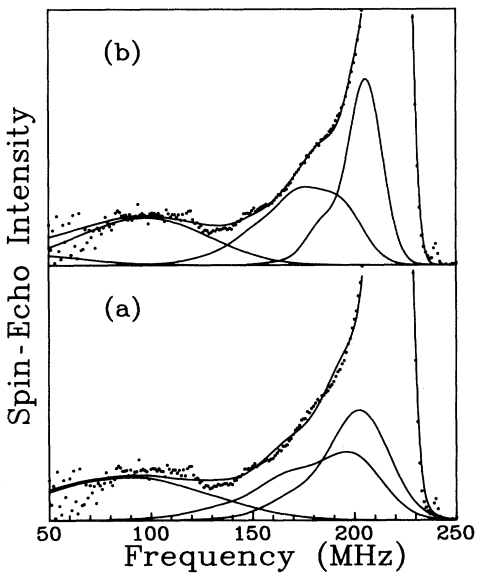

FIG. 7. Modeling of a spectrum showing the contribution of each plane involved in the interface. The gap between the satellites (see text) was either (a) constrained to be equal to the bulk value of 32 MHz or (b) freed (about 20 MHz found by the fit procedure). The bulk contributions are not shown.

concentration, we have chosen first to consider only the Cr concentration in the individual planes. Then, in a second approach and because the concentration-dependent frequency shift is a second and farther neighbor shell effect, we have also considered the average concentration over three planes to represent the local concentration of the middle one. The fit quality is the same for either choice but, of course, the resulting estimated concentration profiles are different.

Since it is difficult to know which set of parameters is the more meaningful, we have computed the concentration profile for the four models we can make with the frequency gap freed or fixed to the alloy value on the one hand, and on the other hand, with the two definitions for the local Cr concentration. The different concentration profiles obtained are given in Fig. 8. It shows that the mixed region is extended over five monolayers per half period. All concentrations do not have the same reliability; indeed, as shown in Fig. 7, the interface spectrum results, within the observation range, from the contribution of three monolayers only: one, the last full Co plane giving rise to a shoulder to the main line; two, the first mixed plane giving rise to the intensity between 200 and 130 MHz; and three, the second mixed plane giving rise to the intensity below 130 MHz. This qualitative result is independent of the set of parameters used, hence the concentrations of the two first mixed planes are directly probed. The third mixed plane does not contribute to the spectrum but it influences the shape and the position of the lines arising from the second mixed plane; the concentration of this third monolayer is thus indirectly probed. It is not possible to determine the concentrations of the two last planes since the spectra give neither direct nor indirect information about them; their maximum and minimum values are fixed to satisfy the constraints of a monotonic concentration profile and a nominal 8 Å Cr-layer thickness. The detailed shape of the concentration profile in Fig. 8 shows that the Cr content is a low 3–7 % in the first mixed plane (depending on the model), then increases rapidly in the second and third mixed plane and saturates in the 50–80 % range in the center of the Cr layer. Actually there is no pure Cr plane in the multilayers.

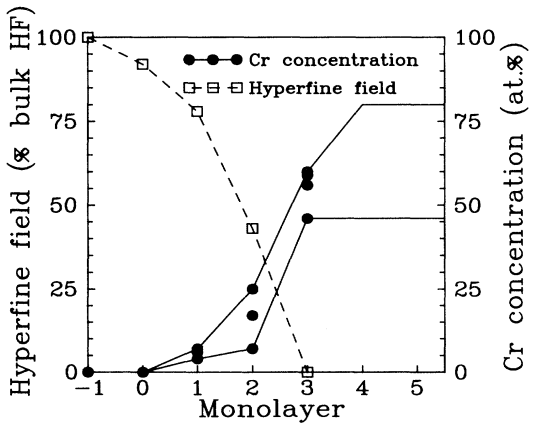

FIG. 8. Cr concentration and average hyperfine field (magnetization) profile in the interface. The monolayer at zero corresponds to the full Co plane which is in contact with the interface. The full lines show the minimum and the maximum monolayer concentration value consistent with our interface model.

As already mentioned, the average (centroid) frequency position and extension of subspectra arising from the last full Co plane and the two first mixed planes are well identified, being weakly dependent on the set of parameters; hence, without referring to the Cr content of these planes, it is possible to have insight on the magnetization profile in the interface. Although the hyperfine field is not fully proportional to the local magnetic moment, its average value provides a reasonable estimate of the average moment. From the centroid of the hyperfine field distribution in each subspectrum, Fig. 8 displays the hyperfine field (magnetization) profile in the interface relative to the bulk hyperfine field (magnetization). From this profile it is possible to deduce that an equivalent of 1.8 Co layers are magnetically dead. This compares with results obtained by the magnetic measurements to be presented in the next section.

B. Magnetic properties

1. Magnetization measurements

The hysteresis loops of all Co/Cr multilayers were measured at room temperature with an applied field parallel and perpendicular to the film plane. Figure 9 shows the magnetization curves of two typical samples, the thickest and the thinnest. Table I summarizes the

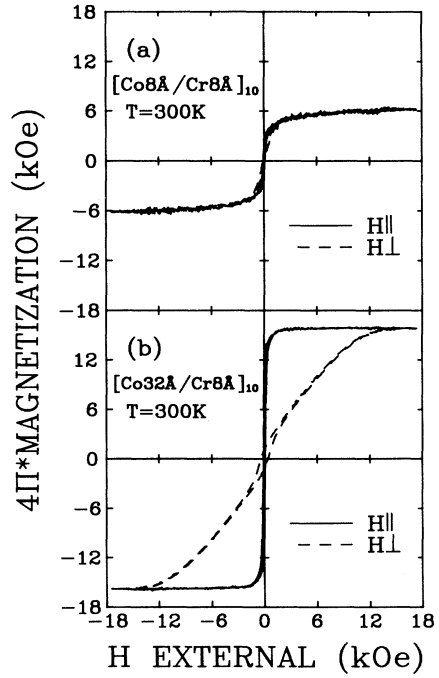

FIG. 9. Hysteresis loops of the (a) [Cr(8 Å)/Co(8 Å)]$_{10}$ and (b) [Cr(8 Å)/Co(32 Å)]$_{10}$ multilayers measured at 300 K with the applied magnetic field parallel (solid curves) and perpendicular (dashed curves) to the film plane.

TABLE I. Magnetic data of the series of [Cr(8 Å)/Co(t_{Co} Å)]$_{10}$ multilayers. M_S^m indicates the measured saturation magnetization and K_{eff} the effective anisotropy per unit volume of Co. The M_S^m/M_S^b ratios deduced from magnetic measurements (VSM) and calculated from the magnetization profile obtained by NMR are given for comparison.

t_{Co} (Å)	M_S^m (emu/cm^3)	K_{eff} (10^6 erg/cm^3)	M_S^m/M_S^b VSM	NMR
8	490	−0.05	0.33	
16	980	−2.02	0.66	0.55
24	1120	−4.20	0.76	0.70
32	1260	−5.93	0.85	0.78

magnetic data of the series of [Cr(8 Å)/Co(t_{Co} Å)]$_{10}$ samples. We note a strong decrease of the measured saturation magnetization values M_S^m, as the Co-layer thickness decreases, from 1260 emu/cm^3 for $t_{Co}=32$ Å to 490 emu/cm^3 for $t_{Co}=8$ Å.

According to previous work, the saturation magnetization of Co is rapidly reduced by the addition of a small amount of Cr. Indeed, zero magnetization is observed in bulk CoCr alloys at about 25 at. % Cr[18,19] and in sputtered films at about 30 at. % Cr.[1,20] Therefore, assuming that the decrease in magnetization from that of the bulk Co is due to Co atoms in an intermixed region, the M_S^m values can be used to estimate the interdiffusion at the interfaces.

A crude approximation consists in dividing the Co layers into two parts: a nonmagnetic part of thickness t_{nm} (dead layers) and a magnetic part having the pure Co saturation magnetization M_S^b. Assuming that t_{nm} and M_S^b are roughly the same from one sample to another, these two parameters can be obtained from the plot of the saturation magnetic moments per unit surface of Co, $M_S^m t_{Co}$, vs Co-layer thickness t_{Co} by a linear fit of the expression (Fig. 10),

$$M_S^m t_{co}=M_S^b\,(t_{Co}-t_{nm})\ .$$

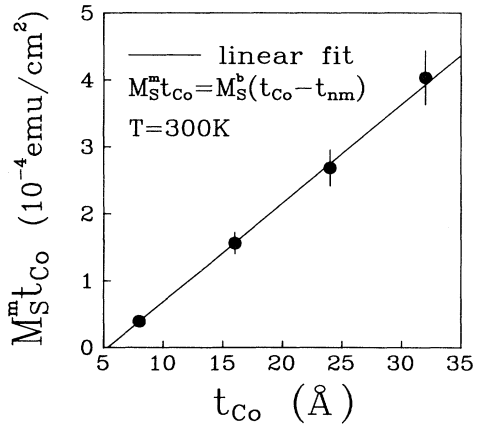

FIG. 10. Variation of the measured saturation magnetic moment per unit surface of Co, $M_s^m t_{Co}$, with the Co-layers thickness t_{Co} for the [Cr(8 Å)/Co(t_{Co} Å)]$_{10}$ multilayers.

Due to uncertainties in the area and thickness of the samples, we estimate that the $M_S^m t_{Co}$ values are known to only 10%. In these conditions, the following values and experimental errors are obtained from the fit: $t_{nm}=5.4\pm1.1$ Å and $M_S^b=1474\pm105$ emu/cm^3. Consequently, the intermixing can be evaluated in terms of 2.7 ± 0.5 dead Co monolayers per Co layer, i.e., 1.4 ± 0.3 dead Co monolayers per interface. This value is smaller than that obtained from the NMR spectra fits and a possible reason for this will be given later. Finally, within experimental error, the calculated pure Co saturation magnetization value is identical to the value quoted for bulk hcp Co that is 1422 emu/cm^3 at room temperature.

To have a more precise idea on the interdiffused thickness, a classical linear interface model can be used. We assume an identical linear composition profile in the Co on Cr and Cr on Co interfaces. A schematic representation of the Co concentration variation with the thickness is given in Fig. 11. Using this model and assuming a linear decrease of the saturation magnetization from that in pure Co, M_S^b, to zero at 25 at % Cr for Co atoms located in the interfaces (see Fig. 11), the measured saturation magnetic moments per unit area of Co should be given by

$$M_S^m t_{Co}=M_S^b(t_{Co}-\tfrac{3}{4}t_i)\ ,$$

where t_i is the average interface thickness. Comparing this expression with that of the linear fit used earlier, we can deduce $t_i=\frac{4}{3}t_{nm}=7.2$ Å. Then, magnetization measurements combined with a linear interface model give an average interface thickness of about four monolayers. This is less than the five monolayers obtained from NMR measurements. An immediate explanation is that the linear magnetization profile proposed here decreases more rapidly in the first Co-rich monolayers than the experimental profile deduced from the spectra fits; this results in an equivalent decrease of the total magnetic moment with a smaller interface thickness.

The linear interface model used for the present estimation of the intermixed thickness assumes that Co on Cr and Cr on Co interfaces are symmetrical. Actually, from our structural study [RHEED analysis, section (i)], this is probably not the case. However, with linear concentration profiles, the total intermixed thickness per Co or Cr

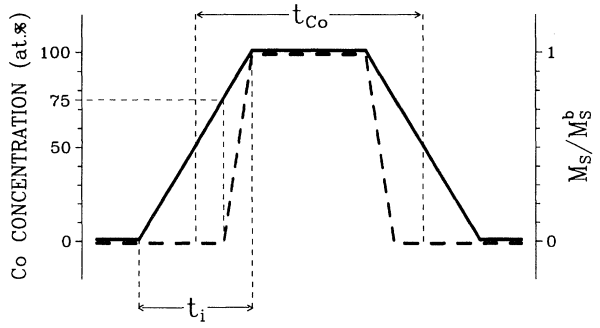

FIG. 11. Co concentration (left scale and solid line) and normalized saturation magnetization (right scale and dashed line) profiles used for the linear interface model.

layer is independent of whether or not the interfaces are symmetrical and is four monolayers in any case. As a result, since the Cr layer thickness is 8 Å, there is certainly no pure Cr monolayer left in our [Cr(8 Å)/Co(t_{Co} Å)]$_{10}$ samples as already has been noticed in the NMR spectra analysis. Moreover, this tends to prove that no pseudomorphism occurs at the Cr on Co interface, the unchanged RHEED patterns being more likely due to interdiffusion.

Let us now compare the measured M_S^m/M_S^b ratios with those calculated from the magnetization profile obtained by NMR. These two series of values are given in Table I. Taking the experimental precision of both techniques into account, there is good agreement between the two series. Nevertheless, one can note that the ratios obtained by VSM are always larger than those deduced from NMR. This could be due to a systematic experimental error which could also partly explain the difference between the two estimates of the equivalent dead Co-layer thickness per interface.

2. *Magnetic anisotropy*

Looking at the hysteresis loops of our Co/Cr samples with equal Cr thickness, it is clear that the difference between parallel and perpendicular saturation fields diminishes when the Co-layer thickness decreases and that it nearly vanishes for $t_{Co}=8$ Å as shown in Fig. 9(a). It is well known that this kind of behavior is due to the existence of a surface anisotropy. Previous works[21–23] have shown that the effective anisotropy per unit volume of ferromagnetic metal, K_{eff}, can be phenomenologically expressed as the sum of a volume and a surface term, i.e.,

$$K_{eff}=K_v+2K_S/t \ ,$$

where t is the ferromagnetic metal layer thickness, K_V is the volume anisotropy per unit volume containing shape, magnetocrystalline, and magnetoelastic contributions, K_S is the surface anisotropy per unit area, and the factor of 2 arises from the two interfaces of each layer. If K_S and K_V are constants, this phenomenological law gives rise to a linear plot of $K_{eff}t$ vs t with a crossover to a perpendicular easy direction ($K_{eff}=0$) at the critical magnetic layer thickness of $-2K_S/K_V$ and a zero-thickness intercept of $2K_S$. If such a phenomenological approach is used for multilayers with diffused interfaces like those in which we are dealing, the volume contribution to $K_{eff}t$ does not originate from the whole magnetic layer any longer but only from that part of it whose volume increases with t, i.e., the pure part. On the other hand, the surface contribution arises from the diffused interfaces ("thick" surfaces) whose volume does not change when increasing t.

Experimental K_{eff} values are obtained from the area between the perpendicular and the parallel magnetization curves, $M_\perp$ and $M_\parallel$:

$$K_{eff}=\int_0^{H_{sat}}(M_\perp-M_\parallel)dH \ ,$$

where H_{sat} is the maximum of the parallel and perpendicular saturation fields. With this expression, K_{eff} is taken to be positive when the preferred orientation for magnetization is perpendicular to the film. Figure 12 shows the plot of the measured effective anisotropy per unit area of Co, $K_{eff}t_{Co}$, vs Co thickness t_{Co}.

For samples with Co layers thicker than 8 Å, the $K_{eff}t_{Co}$ values are negative and roughly follow the linear law noted above. For these multilayers, the anisotropy field is lower than the demagnetizing field and the easy axis remains in the film plane. Fitting the experimental data to the expression $K_{eff}t_{Co}=K_Vt_{Co}+2K_s$, we can deduce a volume anisotropy of $K_v=-9.83\times10^6$ erg/cm^3 and a Co thickness for the crossover between the in-plane and perpendicular easy axis of 13.1 Å. This latter value is close to that obtained by Sato[3] for sputtered Co/Cr multilayers, 12.5 Å. However, for $t_{Co}=8$ Å, the $K_{eff}t_{Co}$ vs t_{Co} plot deviates from the linear law and, although the extrapolated surface anisotropy is strongly positive ($K_S=0.64$ erg/cm^2), a perpendicular easy axis is not obtained. Instead of being clearly positive, the effective anisotropy of the [Cr(8 Å)/Co(8 Å)]$_{10}$ sample is almost nil, which means that the anisotropy field is nearly counterbalanced by the demagnetizing field. For this multilayer, the parallel and perpendicular directions are practically equivalent. This suggests that the switch of magnetization to the normal of the plane would occur for a Co-layer thickness lower but very close to 8 Å. Such a saturation and sometimes even a falloff at small thickness is often observed.[22–24] An explanation for such a kink in the $K_{eff}t$ vs t plot is a change in the growth mode from an incoherent mode, where dislocations release the misfit strains ($t>t_{crit}$), to a coherent one where the lateral lattice planes are in full registry ($t<t_{crit}$).[22,23] In our case, the deviation is more likely related to the bad interface quality and, more precisely, to the intermixing. Indeed, for a series of multilayers with diffused interfaces, the decomposition of the effective anisotropy per unit area as the sum of a volume and a constant surface term is only valid if all samples have the same interfacial topology. In our samples, the equivalent thickness of magnetic metal alloyed in the interfaces has been estimated to be 11 Å in

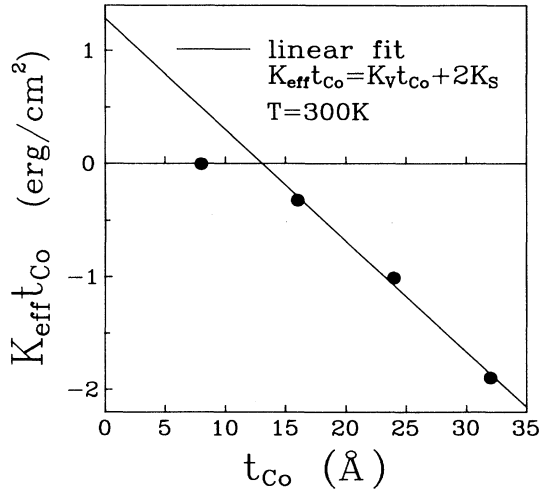

FIG. 12. Dependence of the measured effective anisotropy per surface unit of Co, $K_{eff}t_{Co}$, on the Co thickness t_{Co} for the [Cr(8 Å)/Co(t_{Co} Å)]$_{10}$ multilayers.

each Co layer thicker than 8 Å (NMR). As a consequence, the 8 Å Co layers are not thick enough to exhibit the same concentration profile as the 16, 24, and 32 Å thick Co layers and fulfill the previous condition. In particular, since they contain no pure Co plane, they do not exhibit the transition from pure Co regions to alloyed ones. Then the [Cr(8 Å)/Co(8 Å)]$_{10}$ multilayer has no volume (pure Co) contribution to its effective anisotropy and its surface (interface) anisotropy is certainly different from that of the other samples. In these conditions, the difference between its $K_{\text{eff}}t_{\text{Co}}$ value and that expected from the linear law may be due to a reduction of the surface term arising from the decrease of the concentration gradient in the interfaces.

To conclude this section, let us come back to the K_S and K_V deduced from the linear fit. Despite the large interdiffusion which is likely to reduce the surface anisotropy,[6,7,25] the measured K_S is of the same order as those obtained for different Co/X multilayers (with X=Pt, Au, Cu, Ag, Ir, and Mo) grown by vapor deposition[22] and very close to that measured on MBE-grown Co/Pd multilayers.[26] The K_V value of -9.83×10^6 erg/cm^3 corresponding to the pure Co contribution to K_{eff} is very different from the sum of the shape ($K_D=-12.71\times10^6$ erg/cm^3) and the magnetocrystalline anisotropy ($K_1+K_2=5.52\times10^6$ erg/cm^3) for hcp Co. There are two possible explanations for this difference. The first is the existence of a negative magnetoelastic contribution to K_V resulting from stresses which may arise by the heteroepitaxy of close-packed Co on bcc Cr. The second is a reduction of the pure Co magnetocrystalline anisotropy which may be due to the numerous stacking faults that have been detected in the Co layers: indeed, since fcc Co has a negligible magnetocrystalline anisotropy, a mixing of hcp-like and fcc-like stacking could drastically change the resulting magnetocrystalline contribution to K_V. A magnetoelastic contribution and a reduction of the magnetocrystalline one may also occur together.

IV. CONCLUSION

Using reflection high-energy electron diffraction we have demonstrated an original semiepitaxial growth of Cr on close-packed Co. Kurdjumov-Sachs and Nishiyama-Wassermann epitaxies occur together and give rise to three types of distorted bcc (110) crystallites in the Cr layers. The NMR spectra analysis has shown that the Co layers are neither fcc nor hcp but contain the two kinds of close-packed stackings (*ABA* and *ABC*) which are intimately intermixed. Detailed information on the topology of the interfaces has been obtained by modeling the interfacial part of the NMR spectra. Indeed, we have deduced the average concentration and magnetization profiles in the interfaces and we have evaluated the interdiffusion in terms of 1.8 dead Co monolayers per interface. In the samples with the 16, 24, and 32 Å Co layers, it has been shown that the average thickness of the intermixed region is five monolayers and that there is no pure Cr monolayer left in the 8 Å Cr layers. The large interdiffusion has been confirmed by the magnetization measurements. From the decrease of the saturation magnetization values as the Co-layer thickness diminishes, another estimate of 1.4±0.3 monolayers has been obtained for the dead layer at each interface. Finally, we have attributed the deviation from linearity observed at $t_{\text{Co}}=8$ Å in the thickness dependence of the effective anisotropy per unit surface to the smaller concentration gradient in the interfaces when the Co layers are alloyed to the core.

ACKNOWLEDGMENT

The Institut de Physique et de Chimie des Matériaux de Strasbourg is "Unité Associée au CNRS No. 46."

[1]S. Iwasaki and Y. Nakamura, IEEE Trans. Magn. **MAG-13**, 1272 (1977).
[2]S. Iwasaki and K. Ouchi, IEEE Trans. Magn. **MAG-14**, 849 (1978).
[3]N. Sato, J. Appl. Phys. **61**, 1979 (1987).
[4]M. B. Stearns, C. H. Lee, and T. L. Groy, Phys. Rev. B **40**, 8256 (1989).
[5]P. Boher, F. Giron, P. Houdy, P. Beauvillain, C. Chappert, and P. Veillet, J. Appl. Phys. **70**, 5507 (1991).
[6]F. J. A. den Broeder, D. Kuiper, A. P. van de Mosselaer, and W. Hoving, Phys. Rev. Lett. **60**, 2769 (1988).
[7]H. J. G. Draaisma, F. J. A. den Broeder, and W. J. M. de Jonge, J. Appl. Phys. **63**, 3479 (1988).
[8]D. Stoeffler and F. Gautier (private communication).
[9]G. Wassermann, Arch. Eisenhuttenwes. **16**, 647 (1933).
[10]Z. Nishiyama, Sci. Rep. Tohoku Univ., Ser. 1 **23**, 638 (1934).
[11]G. Kurdjumov and G. Sachs, Z. Phys. **64**, 325 (1930).
[12]Y. Gotoh and H. Fukuda, in *Computer-Aided Innovation of New Materials,* edited by M. Doyoma, T. Suzuki, J. Kihara, and R. Yamamoto (Elsevier, Amsterdam, 1991), p. 843.
[13]J. Dekoster, E. Jedryka, C. Mény, and P. Panissod, J. Magn. Magn. Mater. (to be published).
[14]C. Mény, E. Jedryka and P. Panissod, J. Phys.: Condens. Matter. (to be published).
[15]H. A. M. de Gronckel, K. Kopinga, W. J. M. de Jonge, P. Panissod, J. P. Schillé, and F. J. A. den Broeder, Phys. Rev. B **44**, 9100 (1991).
[16]C. Mény, P. Panissod, and R. Loloee, Phys. Rev. B **45**, 12269 (1992).
[17]M. Kawakami, J. Phys. Soc. Jpn. **40**, 56 (1976).
[18]F. Bolzoni, F. Leccabue, R. Panizzieri, and L. Pareti, J. Magn. Magn. Mater. **31-34**, 845 (1983).
[19]R. D. Fisher, V. S. Au-Yeung, and B. B. Saboo, IEEE Trans. Magn. **MAG-20**, 806 (1984).
[20]S. Iwasaki, IEEE Trans. Magn. **MAG-16**, 71 (1980).
[21]H. J. G. Draaisma, W. J. M. de Jonge, and F. J. A. den Broeder, J. Magn. Magn. Mater. **66**, 351 (1987).
[22]F. J. A. den Broeder, W. Hoving, and P. J. H. Bloemen, J. Magn. Magn. Mater. **93**, 562 (1991).
[23]A. Dinia, K. Ounadjela, A. Arbaoui, G. Suran, D. Muller, and P. Panissod, J. Magn. Magn. Mater. **104-107**, 1871 (1992).
[24]C. H. Lee, H. He, F. J. Lamelas, W. Vavra, C. Uher, and R. Clarke, Phys. Rev. B **42**, 1066 (1991).
[25]P. Bruno, thesis, University of Paris, 1989 (unpublished).
[26]B. N. Engel, C. D. England, R. A. van Leeuwen, M. H. Wiedmann, and C. M. Falco, Phys. Rev. B **67**, 1910 (1991).

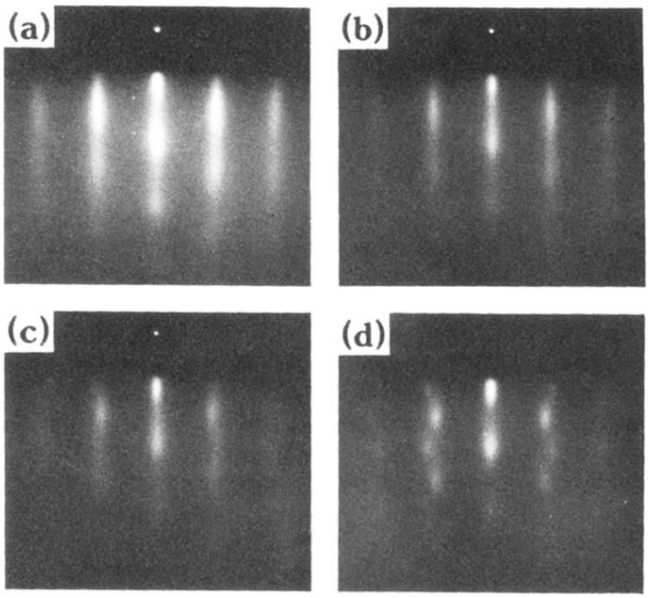

FIG. 1. Evolution of the RHEED patterns observed along the [$11\bar{2}0$] direction of a (0001) Co surface during the growth of a 30 Å Cr layer: (a) (0001) Co surface before Cr growth; (b) the pattern is unchanged after 2 Å Cr; (c) a streak splitting clearly appears after 6 Å Cr; (d) the splitting reaches a stable value for a Cr layer thicker than 12 Å.